*Q. J. R. Meteorol. Soc.* (2002), **128**, pp. 1–999 doi: 10.1256/qj.02.169

# Large eddy simulation of atmospheric convection on Mars

By TIMOTHY I. MICHAELS* and SCOT C. R. RAFKIN
*Southwest Research Institute, USA*

(Received 1 January 2000; revised 31 January 2001)

SUMMARY

Large Eddy Simulations are performed using the Mars Regional Atmospheric Modeling System (a non-hydrostatic, mesoscale model) in order to obtain a detailed, three-dimensional understanding of the daytime Mars atmospheric boundary layer. These microscale runs utilize the full radiative transfer (including a static dust profile) routines of the mesoscale model and a multi-level, prognostic subsurface thermal model. Surface albedo, thermal inertia, Coriolis parameter, and solar forcing are homogeneously set to values at the Mars Pathfinder landing site {19.33°N, 33.55°W (IAU1991); $L_s$ = 143°}. The initial state is obtained from a previous mesoscale simulation, and is representative of the Mars Pathfinder landing site during summer.

The convective boundary layer of Mars is found to exhibit structures and turbulent statistics outwardly similar to that of Earth's convective boundary layer. However, direct infrared radiative heating of the near-surface atmosphere is the primary mechanism for the transfer of energy from the solar-heated surface, and affects the behaviour of the convection. Mars convection is more intense than that on Earth, primarily due to lesser gravity and atmospheric mass. Also, certain empirical scaling constants within the subgrid-scale turbulence parametrization (originally developed for terrestrial Large Eddy Simulations) appear to require significant reduction in order for the scheme to perform adequately on Mars. The simulation results are used to further meaningfully interpret spacecraft images of convective clouds. The results also compare favourably with Mars Pathfinder *in situ* meteorological measurements, and help reconcile large daytime variances in that dataset.

KEYWORDS: Convective boundary layer Dust devils Subgrid-scale turbulence parametrization

## 1. INTRODUCTION

The structure and dynamics of the Mars atmospheric boundary layer (ABL) are neither well known nor well understood. However, the complex processes and motions within this lowest region of the atmosphere directly impact the descent and landed phases of all surface-based Mars missions, regardless of whether they are robotic or manned. Furthermore, the processes that cause aeolian erosion of landforms, raise and redeposit dust, and allow for the surface deposition and sublimation of water and carbon dioxide ices all occur within the ABL. This region of the atmosphere also provides a primary energy conduit through which solar energy drives the large-scale general circulation. Thus it appears that investigation of the Martian ABL is well-warranted. A summary of past work and the current state of knowledge pertaining to this topic follows.

### (*a*) *Spacecraft measurements*

The twin Viking Lander spacecraft provided the first *in situ* measurements of the near-surface Mars atmosphere in 1976. This data was examined by Sutton *et al.* (1978), who concluded that the likely daytime ABL, or convective boundary layer (CBL), depth at the Viking 1 Lander site during summer is 4-5 km, the maximum daytime surface sensible heat flux is 15-20 W m$^{-2}$, and low-level convection is three times as vigorous as its terrestrial counterpart. Although the results of such studies are important and quite useful, one must not lose sight of the fact that such quantities are very difficult to measure, even on Earth, and that many assumptions and/or approximations (e.g., surface temperature determination method, use of scaling laws developed for Earth, instrument uncertainties, etc.) were made in order to indirectly arrive at these quantities. Other Viking-era evidence of Mars CBL depth and structure includes large dust devils up to

* Corresponding author: Southwest Research Institute, 1050 Walnut St, Suite 400, Boulder, CO 80302, USA.

7 km in height (Thomas and Gierasch 1985) and convective cloud streets (Briggs *et al.* 1977) captured in Viking Orbiter spacecraft imagery.

Mars Pathfinder (MPF) collected in 1997 the most recent and highest temporal resolution *in situ* dataset yet. MPF results (Schofield *et al.* 1997) confirmed the presence of strong near-surface temperature gradients, chronicled the passage of dust devils and other convective structures over the lander, and suggested that the turbulent power spectrum of Mars' atmosphere is similar to that of Earth in some conditions. Also, small (on the order of 100 m in diameter) nearby dust devils were discovered in MPF imagery (Metzger *et al.* 1999), offering yet another clue to the structure of the Mars CBL.

Recent imagery from the Mars Orbiter Camera (MOC) aboard the Mars Global Surveyor (MGS) spacecraft has improved our indirect knowledge of the CBL. Several intermediate-size dust devils have been imaged by MOC at high resolution. Numerous dust devil tracks are visible on much of the planet's surface, often exhibiting complex loops and turns that are indicative of the dynamical CBL processes that the phenomena were embedded in (Malin and Edgett 2001). Convective cloud streets have been imaged in greater detail than before (Wang and Ingersoll 2002). Convective structures are even revealed in detailed MOC images of dust plumes. These data only offer hints at the nature of the CBL, as it remains invisible for the most part.

### (*b*) *Analytical and numerical modeling studies*

The work of Goody and Belton (1967) implied that Mars might have a relatively deep ABL compared to that of Earth (the terrestrial ABL depth is typically 1-3 km), owing to the short radiative time constant of the Martian atmosphere. A one-dimensional (1-D) analytical and numerical study conducted by Blumsack *et al.* (1973) concluded that the daytime ABL (also known as the convective boundary layer, or CBL) on Mars is likely 3-15 km in depth. It was emphasized that the gross ABL structure appears to be controlled primarily by the radiative heating of the lowest few kilometers due to upwelling infrared energy from the surface {further supported by the later work of Haberle *et al.* (1993) and Savijärvi (1991)}. An early three-dimensional (3-D) Mars general circulation model (without direct solar heating of suspended dust) attained a maximum CBL depth of 6-8 km (Pollack *et al.* 1976).

Ye *et al.* (1990) applied improved analytical techniques and two-dimensional (2-D) numerical modeling to the problem, and concluded that the Martian CBL is likely 3-4 times deeper, has a smaller daytime surface sensible heat flux (15-30 W m$^{-2}$), and exhibits a representative eddy mixing coefficient ten times larger (i.e., convection is more vigorous) than the terrestrial CBL. Subsequent modeling studies using various one-, two- and three-dimensional numerical models (Savijärvi and Siili 1993; Haberle *et al.* 1993; Savijärvi 1995) yielded values similar to the Viking results. Model simulations of the Mars Pathfinder atmosphere attained CBL depths of 4-5 km and satisfactorily simulated the near-surface temperature measurements (Savijärvi 1999; Haberle *et al.* 1999).

However, it must be noted that the above work was carried out using surface layer theories and largely empirical bulk turbulence parametrizations developed for Earth's atmosphere. It has not been rigorously shown that these methods are universal for all atmospheres similar to the terrestrial one (e.g., Mars' atmosphere). Furthermore, these parametrizations often do not accurately reflect the detailed effects of CBL turbulence, even on Earth. In order to examine the Mars CBL with the least practical amount of parametrization and thus presumably with less error, a Large Eddy Simulation (LES) may be performed. The LES method attempts to explicitly resolve all of the important, larger turbulent motions that transport the vast majority of energy in the CBL, while parametrizing the small turbulent motions that primarily act to diffuse and dissipate energy.

The pioneering terrestrial LES work was by Deardorff (1972). That first investigation compared relatively well with available observations. However, computational power proved to be a severely limiting factor, and little additional numerical work was published until the mid-1980s, when computers had improved sufficiently. By the close of that decade, the primary structure of the convective boundary layer had been described in detail (Schmidt and Schumann 1989), though there are a paucity of observations to compare those results to. Briefly, the buoyantly-driven ABL is seen to develop quasi-steady cellular updraught/downdraught structures, roughly hexagonal in shape, with narrow, intense updraughts surrounding much wider and less intense downdraughts. As computer capability continued to improve, additional investigations were conducted, such as comparing shear- and buoyancy-driven ABLs (Moeng and Sullivan 1994). The widening of the cellular structures with time in LES has been noted by Fiedler and Khairoutdinov (1994) and Dörnbrack (1997). Recently, Kanak *et al.* (2000) has laid the groundwork for the numerical investigation of small-scale vortices in the Earth's CBL (e.g., dust devils). Also, the terrestrial version of the model modified (for Mars) for use in this study has been used successfully for LES (e.g., Hadfield *et al.* 1991; Walko *et al.* 1992).

Studies of the Mars atmosphere using a 2-D LES (Odaka *et al.* 1998; Odaka 2001) predict vigorous turbulent mixing to a depth of approximately 10 km in the Mars CBL. A previous 3-D LES simulation using an early version of the Mars Regional Atmospheric Modeling System (MRAMS) predicted a maximum CBL depth of 7 km, quite vigorous convection, and possible dust devil circulations (Rafkin *et al.* 2001). At the time of writing, there are no other independently published 3-D Mars LES works.

### (*c*) *Current state of knowledge and the present approach*

Based on results and conclusions from previous work, the overall consensus appears to be the following: The maximum depth of the Mars CBL varies with season and location but generally is in the range of 3-8 km. Dust devils appear to be ubiquitous at many scales in the CBL, and can be several times larger than their terrestrial counterparts. Convective cloud streets appear to be similar to those associated with Earth's CBL, implying that the overall structure of Mars convection is similar as well. Turbulence is more vigorous due in part to the lesser gravity and thin atmosphere of Mars. There exist present-day mechanisms for lifting dust in the Mars CBL, proven in part by the existence of dust devils, their tracks on the surface, and the non-permanence of those tracks. Radiative heating of the lowest kilometer of the atmosphere is likely an important mechanism in the Mars CBL, and contrasts strongly with the heating mechanism of the Earth CBL. Surface layer theories developed for Earth appear to be valid (or at least similar) for Mars as well, according to MPF measurements (Schofield *et al.* 1997).

The present study is undertaken to simulate and investigate the three-dimensional processes and structure of the Mars CBL using MRAMS large eddy simulations. This study has the following three goals:

(1) Determine the three-dimensional structure of the Mars CBL under low wind-shear conditions, and compare with the structure of the Earth's CBL.

(2) Quantify the turbulent statistics of the 3-D Mars CBL.

(3) Compare LES results with spacecraft measurements and images, in order to gain confidence in the model solution and offer insight on how to more fully interpret those data.

## 2. Methodology

### (*a*) *Numerical model description*

The model employed in this study is the Mars Regional Atmospheric Modeling System. In brief, MRAMS is a non-hydrostatic, finite-difference, limited domain (with optional nested domains), mesoscale model designed to simulate the atmosphere of Mars. It is an improved version of the model described and used by Rafkin *et al.* (2001). Details pertaining to the recent model modifications may be found in Michaels (2002). For the present purpose, however, only the modifications made to the subgrid-scale (SGS) turbulence parametrization used in the LES are relevant.

The SGS turbulence model used in the present study is a modified form of the 1.5 order, prognostic SGS turbulent kinetic energy (TKE or $e$) scheme described by Deardorff (1980). This particular SGS parametrization was chosen because it had already been implemented and successfully utilized in the terrestrial version of MRAMS (RAMS; e.g., Walko *et al.* 1992). The prognostic equation for the variation of $e$ with time may be written schematically as

$$\frac{\partial e}{\partial t} = (-ADV - TURB) + BUOY - SHEAR - \varepsilon \, . \tag{1}$$

The buoyant production/consumption and mechanical (or shear) production/loss terms are respectively defined according to

$$BUOY = -K_{\mathrm{h,V}} N^2 = -K_{\mathrm{h,V}} \frac{g}{\theta} \frac{\partial \theta}{\partial z} \ , \tag{2}$$

$$SHEAR = \frac{\partial u_i}{\partial x_j} \left\{ -K_{\mathrm{m,A}} \left( \frac{\partial u_i}{\partial x_j} + \frac{\partial u_j}{\partial x_i} \right) + \frac{2}{3} \delta_{ij} e \right\} \ , \tag{3}$$

where $N^2$ is the Brunt-Väisälä frequency, $g$ is the surface gravitational acceleration, $\theta$ is the atmospheric potential temperature, $u_i$ are the velocity components in the three coordinate directions $x_i$ ($i$ = 1, 2, 3), $\delta_{ij}$ is the Kronecker symbol, and $K_{\Box}$ are the mixing coefficients (defined later in this section).

Deardorff's original scheme performs best on a computational grid that is isotropic in all three spatial dimensions (i.e., the grid spacing is equal in all directions). The main reason for this isotropic dependence lies in the definition of a subgrid-scale mixing length. Deardorff defines this mixing length as the cube root of the product of the $x$-, $y$-, and $z$-direction grid spacings ($\Delta x$, $\Delta y$, $\Delta z$). However, for the Martian LES it was deemed necessary to have a stretched vertical grid to reduce computational expense. An alternative approach better able to handle vertical grid anisotropy is to define two subgrid-scale mixing lengths: one for the horizontal directions ($\ell_{\mathrm{H}}$), and another for the vertical direction ($\ell_{\mathrm{V}}$), according to

$$\ell_1 = \beta_1 \Delta x \ , \quad \ell_2 = \beta_2 \Delta y \ , \quad \text{and} \ \ \ell_1 = \ell_2 = \ell \ , \quad \beta_1 = \beta_2 = \beta \ , \tag{4}$$

$$\ell_3 = \max\{0.7\ell \ , \ (\ell^2 \beta_3 \Delta z)^{1/3}\} \ , \quad \ell_{\mathrm{s}} = 0.76 N^{-1} e^{1/2} \ , \tag{5}$$

$$\ell_{\mathrm{H}} = \begin{cases} \ell & \text{if } N^2 \leq 0 \text{ (unstable or neutral)} \\ \min(\ell, \ell_{\mathrm{s}}) & \text{if } N^2 > 0 \text{ (stable)} \end{cases} \ , \tag{6}$$

$$\ell_{\rm V} = \begin{cases} \ell_3 & \text{if } N^2 \leq 0 \text{ (unstable or neutral)} \\ \min(\ell_3, \ell_{\rm s}) & \text{if } N^2 > 0 \text{ (stable)} \end{cases} , \tag{7}$$

where $\beta$ and $\beta_3$ are scaling constants (discussed in more detail later in this section). The lower limit for $\ell_3$ (Eq. 5) was chosen arbitrarily to prevent the vertical mixing from being insufficient where $\Delta z$ is small (near the surface).

The SGS mixing lengths defined above are used with the turbulent Prandtl number ($Pr$) to calculate the mixing coefficients for horizontal momentum, horizontal scalars, average momentum, vertical momentum, and vertical scalars,

$$K_{\rm m,H} = K_{\rm h,H} = 0.1e^{1/2}\ell_{\rm H} \ , \quad K_{\rm m,A} = 0.1e^{1/2}(\ell_{\rm H}\ell_{\rm H}\ell_{\rm V})^{1/3} \ , \tag{8}$$

$$K_{\rm m,V} = 0.1\ell_{\rm V}e^{1/2} \ , \quad K_{\rm h,V} = K_{\rm m,V}/Pr = K_{\rm m,V}\{1 + 2(\ell_{\rm V}/\ell_3)\} \ , \tag{9}$$

respectively. Note that in the shear term of the prognostic calculation of subgrid-scale TKE (Eq. 3), Deardorff's definition of the mixing length is retained (within $K_{\rm m,A}$), since it does contain information (however muted) about the full dimensions of each grid cube.

Viscous dissipation ($\varepsilon$) is parametrized by

$$\varepsilon = C\frac{e^{3/2}}{(\ell_{\rm H}\ell_{\rm H}\ell_{\rm V})^{1/3}} \ , \quad \text{where } C = 0.19 + 0.51\left(\frac{\ell_{\rm H}\ell_{\rm H}\ell_{\rm V}}{\ell_1\ell_2\ell_3}\right)^{1/3} , \tag{10}$$

except in the lowest model layer (nearest the surface) where $C = 3.9$, as suggested in Deardorff (1980) and elsewhere to better handle "wall effects". $ADV$ is the 3-D advection of $e$ by the resolved-scale wind, and $TURB$ is primarily the subgrid-scale transport (diffusion; uses the mixing coefficients given above) of $e$ by small turbulent eddies (also implicitly includes the "pressure correlation" term of the full TKE tendency equation). The latter two terms are calculated outside of the SGS model (detailed in Rafkin *et al.* 2001).

It was found through preliminary numerical experiments that the values for the scaling constants ($\beta$ and $\beta_3$), which in practice have a value equal to or slightly greater than unity on Earth, needed to be decreased by a factor of at least three (scaling constants used in this work are $\beta = 0.17$, $\beta_3 = 0.15$) in order to avoid overdiffusing (i.e., no convective motions are able to develop at any time during the day) the model solution for Mars. If the scaling constants (and thus ultimately the mixing coefficients) are too large, resolved-scale convection fails to initiate, and instead a very quiescent ABL develops due solely to the accumulated action of subgrid-scale diffusion. If the scaling constants are made too small, numerical noise ("$2\Delta x$" noise) quickly develops and dominates the model solution. Many combinations of scaling values were tried, including pairs where $\beta_3$ was much greater than $\beta$, and vice versa. It was found that the horizontal scaling constant ($\beta$) effectively controlled the timing of the onset of resolved-scale convection and the damping of numerical noise. In stark contrast, the model solution appeared to be much less sensitive to the value given to the vertical scaling constant. The significance of these observations is uncertain.

### (*b*) *Numerical experiment design*

Two separate LES were performed at different horizontal and vertical resolutions. This was done in order to better understand the impact of model grid spacing on the resulting solution, to attempt to resolve convective structures more clearly, and to elucidate the characteristics of the flow at and during the onset of ABL convection.

Both simulations were initialized in exactly the same manner, and used the same model physics and parametrizations. However, due to finite time and computational resources, the computational grids of the simulations were not the same size, nor were they integrated over the same period of time.

The computational grid of Simulation 1 (hereafter referred to as S150) is 24×24 km in the horizontal and approximately 9.5 km deep in the vertical. The horizontal grid spacing is 150 m, and was chosen based on earlier two- and three-dimensional trial runs that indicated this value to be satisfactory for modeling the largest CBL eddies. The vertical grid was gradually stretched with height, with a first layer thickness of 4 m (lowest level at about 1.9 m above the surface), increasing to a maximum of 225 m (1.5 times the horizontal grid spacing, in order to keep the bulk of the three-dimensional computational grid approximately isotropic) aloft. These dimensions require 160×160×61 grid points. The rationale for choosing the above grid dimensions is that Mason (1989) postulated that a grid at least 3.2 times the width of an individual convective cell was necessary to properly represent CBL statistics on Earth. Based on earlier tests (which suggested that Martian convective cells were 7 to 8 km wide) and computer limitations (both memory/storage and computational time needed), the above dimensions were chosen – with the aim of having significant CBL statistics and realistic CBL structures and dynamics.

The computational grid of Simulation 2 (hereafter referred to as S30) is 6×6 km in the horizontal and approximately 2.3 km deep in the vertical. The horizontal grid spacing is 30 m. The vertical grid is gradually stretched with height, with a first layer thickness of 4 m (lowest level at about 1.9 m above the surface), increasing to a maximum of 45 m aloft. These dimensions require 200×200×61 grid points.

All grids were made strictly Cartesian (i.e., no attention was paid to planetary curvature). Flat topography was assumed (i.e., topography was set to zero meters everywhere). The entire domain of each simulation was assumed to be at the location of the Mars Pathfinder landing site at the southern edge of Chryse Planitia {19.33°N, 33.55°W (IAU1991 areographic coordinate system)} for the purpose of radiative computations. This also allows for a more meaningful comparison with actual landed MPF data. Thermal inertia and albedo were set to be constant over the entire grid (set to representative values from the MPF site: thermal inertia = 384.5 J $K^{-1}$ $m^{-2}$ $s^{-1/2}$, albedo = 0.197). The surface aerodynamic roughness length used was 0.03 meters. A static dust distribution was used (dust concentration decreased roughly exponentially with height), with a dust optical depth of 0.3 on a pressure surface of 6.1 hPa.

Cyclic (sometimes termed periodic) lateral boundary conditions were used for both simulations, and effectively simulate an infinite planar domain. This type of boundary condition was primarily chosen because there are no three-dimensional ABL observations for Mars to use as boundary conditions and an appropriate mesoscale simulation to provide boundary conditions was judged to be too time-intensive to undertake at present. Moreover, it is likely a reasonably good approximation to the situation in the northern plains of Mars. Assuming a mean wind of 5 m $s^{-1}$, the equivalent domain simulated during a solar convective day of 10 Mars-hours (about 36990 s) is basically a flat plain 200 km wide with atmospheric convection occurring everywhere. A plain of such a size is easily found near the MPF landing site. At the model top, a Rayleigh friction layer 5 vertical grid points thick was used with a dissipation time-scale of one Mars-hour.

The Coriolis parameter was kept spatially constant (set to the value at 19.33°N) for both simulations. The full subsurface thermal model of MRAMS was used, as well as the full radiation code (from the NASA Ames Mars general circulation model;

includes dust and carbon dioxide gas plane-parallel radiative transfer at visible/near-infrared wavelengths and in two infrared ranges). However, the use of cyclic boundary conditions necessitated that the solar zenith angle be treated as if the entire grid was a single point (the areographical location of the grid center). A radiative time step of 30 s was used in an attempt to capture the radiative changes induced by the largest convective ABL eddies (since they may significantly alter the temperature/pressure profile over that period of time). The starting season was approximately $L_s = 143°$, which is the latter portion of the Northern Hemisphere summer. This season was chosen partly because the synoptic scale disturbances should be weak at the MPF site (allowing for approximate atmospheric repeatability sol after sol), and secondly, this was the season that the Mars Pathfinder spacecraft landed at, so the model results should compare well with the landed observations.

Both simulations were initialized with a single sounding from a previous mesoscale simulation of the MPF site. The initial fields were thus horizontally homogeneous. Only the sounding temperature and pressure profiles were used. Wind components were specified as follows: $u$ = 5 m s$^{-1}$, $v$ = 0 m s$^{-1}$, and $w$ = 0 m s$^{-1}$. Although there is no initial wind shear, after the simulation begins friction with the surface quickly produces weak shear throughout the lowest several hundred meters of the CBL. This choice was made in order to examine the intrinsic structure (i.e., the weakly sheared structure) of the convective boundary layer on Mars, but still have a slight amount of mean wind in one direction to move the convective cells/phenomena across the domain (which adds realism). The horizontally homogeneous potential temperature field from the sounding was randomly perturbed by up to 0.1 K at the lowest model level in order to provide a slight amount of inhomogeneity to foster the onset of resolved convection.

Two generic 24 Mars-hour time systems are used in this work. The first, analogous to the terrestrial Coordinated Universal Time (UTC) system and shares the same name, defines 0000 UTC to be midnight at the 0°E meridian in the IAU1991 areographic coordinate system. The second, Local Solar Time (LST), is offset from UTC by a simple linear function of areographic longitude analogous to local time on Earth. Both simulations were started at 0810 UTC (about 0556 LST), which is just after the local sunrise, in order to simulate the entire convective ABL evolution (achieved only in S150).

A dynamical time step of 2 s was required to keep S150 numerically stable after resolved convection initiated, due to large vertical velocities across the relatively thin model layers near the surface. A fully three-dimensional snapshot of all prognostic variables was archived every 300 simulated seconds. S150 was halted at 2020 UTC (1805 LST, 45000 s after start) after the ABL convection had almost completely dissipated. Similarly, a dynamical time step of 1 s was required to keep S30 numerically stable. Model output occurred every 180 s. S30 was halted at 1349 UTC (1134 LST, 20880 s after start) after it was judged that the convective cells were becoming too large for the grid.

## 3. Results

### (*a*) *Spatial and dynamic CBL structure*

(i) *Convective cells.* Loss of momentum to the ground (due to friction) quickly creates near-surface speed shear in the initially vertically homogeneous wind profile. Soon after, the surface/air interface becomes warmer than the immediately overlying air (due to insolation), and atmospheric convection ensues (as the fluid's natural way to cool its lower boundary). The convective boundary layer initially evolves purely due to subgrid-scale (SGS) turbulence, evidenced by a deepening layer of greatly increased SGS turbulent kinetic energy (the only SGS quantity truly prognosed by the model) bounded by the surface and having no resolved spatial perturbations in wind, temperature, or pressure. When this SGS CBL attains a depth roughly equal to three times the horizontal grid spacing, resolved-scale convection initiates and immediately dominates the SGS processes (by an order of magnitude or more in terms of turbulent energy fluxes). This disparity between the magnitude of the SGS and resolved-scale fluxes at nearly the same time of sol is noteworthy, as it suggests that the SGS parametrization is not adequately representing the real-world SGS turbulence intensity (discussed further in Section 3b). The CBL depth at which this transition takes place is strongly a function of the strength of the horizontal SGS diffusion in the model. SGS diffusion was tuned to initiate resolved-scale convection at approximately three times the horizontal grid spacing since the model cannot properly treat turbulent eddies smaller than that (assuming the said eddies are all quasi-isotropic).

Resolved-scale convection begins as regularly spaced linear plumes of buoyant fluid aligned parallel to the mean shear vector (Fig. 1a). Note that updraughts and downdraughts occupy equal areas and have roughly equal magnitudes at this stage. However, in a near-surface (i.e., where there is vertical speed shear due to friction) environment dominated by buoyant forces, rather than shear forces, such linear structures are not stable. In order to maintain such symmetric structures, the three-dimensional fluid flow must somehow maintain an excruciating spatial symmetry, since any asymmetries will tend to amplify (because of momentum transport from aloft) or at least produce other asymmetries in the flow. In the model solutions, the first returning fluid (i.e., fluid that has journeyed upwards in one of the initial updraughts and has now returned to the surface in a downdraught) exhibits spatial asymmetries in vorticity (generated along the updraught lines), momentum, and heat (perhaps in part caused by gravity wave interactions along the upper boundary of the CBL) that warps sections of the linear updraught/downdraught structures in directions roughly perpendicular to the mean shear vector. The warping causes sections of adjacent updraught structures to connect, forming elongated, closed loop updraught structures. As this process continues, the linear updraught structures give way to roughly elliptical structures (Fig. 1b), which in turn divide into roughly circular structures (Fig. 1c). Also, downdraughts gradually encompass much more area and become weaker than updraughts. Finally, updraught strength increases dramatically during this period, as insolation, and thus the heating of the lower boundary of the atmosphere (most importantly due to absorption of upwelling infrared radiation, and secondarily due to molecular thermal conduction from the surface) increases. The shape of the approximately circular convective structures, or cells, is often more aptly described as polygonal (chiefly quadrilateral, pentagonal, and hexagonal). These polygonal cells persist throughout the remainder of the solar convective day.

The structure of these polygonal convective cells is startlingly complex and efficient. Every cell side is shared with an adjoining cell, so that there is no surface area left unencompassed. The cell sides are composed of relatively narrow and intense updraughts, while the majority of the cell interior contains only broad, relatively weak downdraughts. The lowest several hundred meters of each cell interior is a region of divergent flow towards the cell sides. Embedded in this low-level flow are much smaller convective cells with a structure similar to their larger cousins. This smaller-scale convection, kept from growing larger by subsidence and shear due to descending air in the large-scale cell interior, serves to channel near-surface buoyant fluid from the interior of the cell outward to feed the larger-scale updraughts that make up the cell sides.

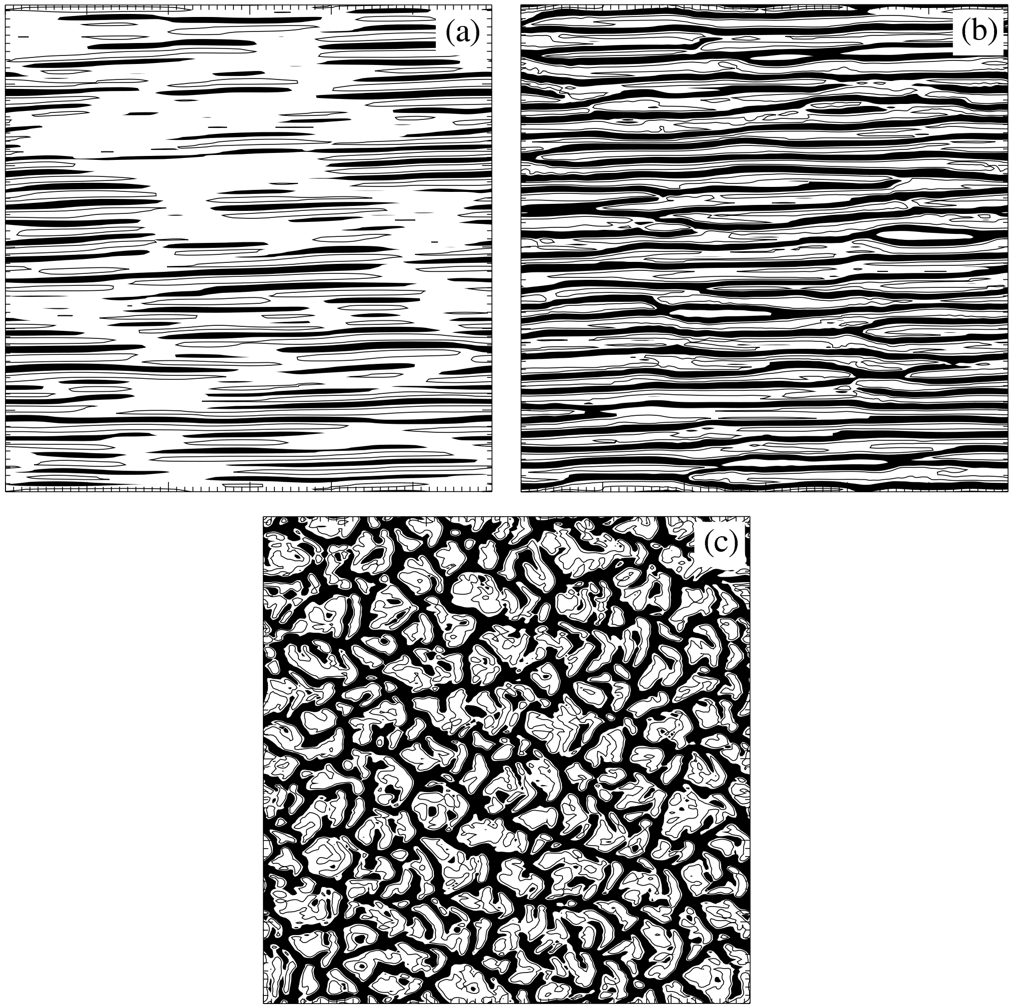


Figure 1. Horizontal cross-sections (each 6×6 km; $y$ is vertical axis, $x$ is horizontal axis) of S30 vertical velocity {filled areas are regions of upward (positive) velocity} at $z$ = 25.4 m for: (a) 0749 LST, initiation of resolved-scale convection, with contours at -0.01 and 0.01 m $s^{-1}$; (b) 0804 LST, warping of linear convective features, with contours at -0.2 and 0.1 m $s^{-1}$; and (c) 0833 LST, early polygonal convective cells, with contours at -0.2 and 0.1 m $s^{-1}$.

The Mars Orbiter Camera (MOC) aboard the Mars Global Surveyor (MGS) spacecraft has frequently imaged what appear to be convective clouds over the Syria Planum region of Mars (Wang and Ingersoll 2002). Figure 2a is a 48×48 km portion of such a MOC image (M0104901, taken at approximately 1430 LST). Comparing the overall shapes and distribution of the white cloud areas in Fig. 2a with the contoured areas (regions of strong vertical velocity near the top of the S150 CBL at 1441 LST) of Fig. 2b, there are striking similarities that appear to further confirm (albeit indirectly) the nature of these clouds, as well as providing a real-world partial validation of the LES results (i.e., that regions of the Mars atmosphere exhibit convection of similar scale and structure as the simulation). The approximate size, height (compared to cloud heights estimated from cast shadows), spatial distribution, and lobed nature of the simulated

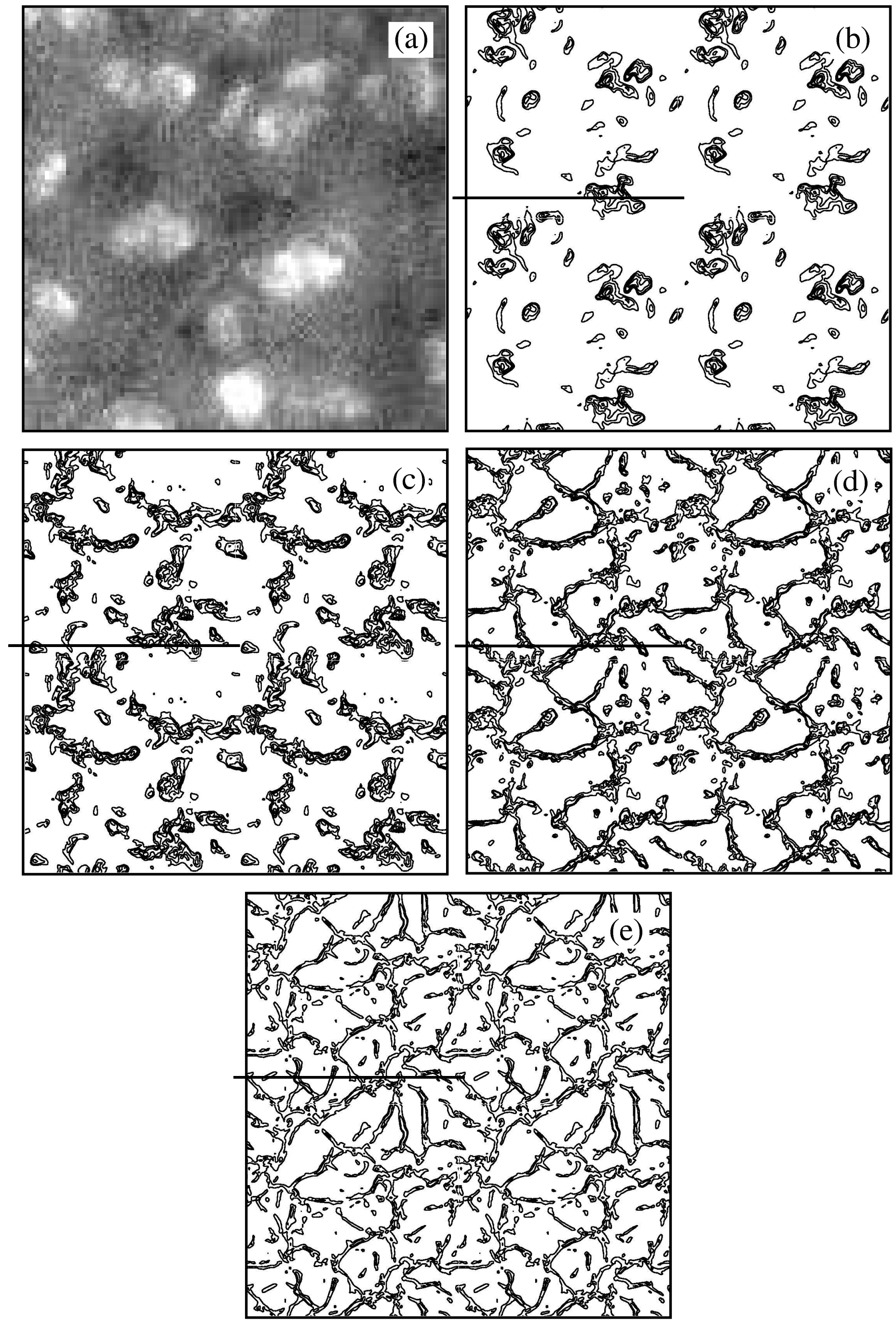


Figure 2. (a) Area (48×48 km) of presumed convective clouds over Syria Planum (portion of Mars Orbiter Camera image M0104901). Horizontal cross-sections (4 copies tiled to create an area of 48×48 km) of S150 vertical velocity (filled areas are regions of velocity greater than 2 m s$^{-1}$) at 1441 LST and: (b) $z$ = 4342 m; (c) $z$ = 2092 m; (d) $z$ = 988 m; and (e) $z$ = 385 m. Straight solid line in above horizontal sections indicates the location of the vertical cross-section shown in Fig. 3 below.

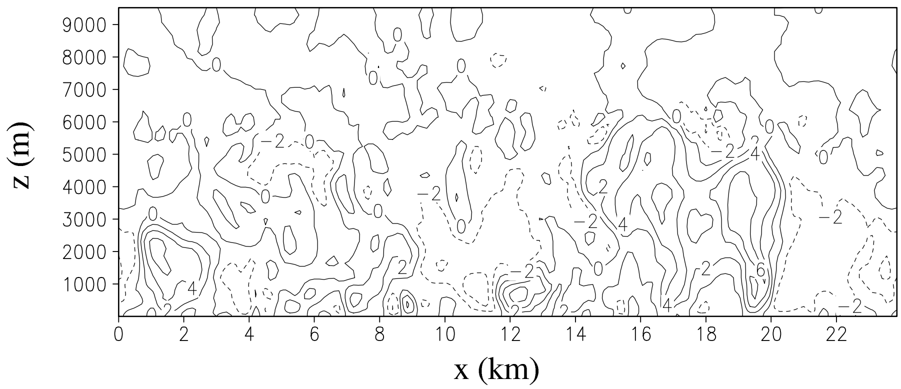


Figure 3. Vertical (X-Z) cross-section of vertical velocity through the S150 domain (location indicated in Figs. 2b-e by straight solid line) 1441 LST. The contour interval is 2 m $s^{-1}$, and dashed contours indicate negative (descending) velocities.

updraught cores all compare well with the MOC image. These clouds' morphology and formation mechanism are quite similar to terrestrial "open" cellular convective clouds (Atkinson and Zhang 1996) that occur over warm ocean surfaces during cold-air outbreaks. A notable difference is that in the relatively dry atmosphere of Mars, condensation is only able to occur above the very strongest updraughts (at the vertices of the cellular structure), whereas the terrestrial cellular clouds are often seen to trace the outline of the entire convective cell (not just the vertices), due to abundant water vapor.

The numerical simulation results provide detailed representative information about atmospheric structure invisible in the spacecraft image. Figure 2c shows the updraughts organized into large convective cells mid-way through the CBL (2092 m). Updraught intensity within the cell walls is not uniform. Descending to 988 m, Fig. 2d illustrates how the convective cells become smaller and more distinct, and their constituent updraughts narrower (and also less intense) near the surface. At a height of 385 m (Fig. 2e), a multitude of small, rapidly changing updraught structures are present, transporting highly buoyant fluid away from the surface. A west-to-east vertical cross-section (of vertical velocity) through the domain at the same time is shown in Fig. 3. The proportions of this fi gure are 1:1 (i.e., no vertical exaggeration). Several deep updraughts are visible, along with shallow updraughts and the broad downdraughts.

The mean size of all scales of convective cells broadens continuously throughout the day. This occurs at a pace dictated by the current available insolation and vertical temperature and momentum structure of the atmosphere (i.e., the cells may broaden very rapidly if a marginally stable layer of the atmosphere lies above them or if a layer of heightened momentum aloft is encountered and is then brought down to the surface). The overall mechanism that causes the cells to broaden appears to be simply conservation of mass (i.e., if there is more mass going up per unit time, there should also be correspondingly more mass per unit time descending to take its place, and vice versa).

Figure 4a shows the mean (averaged over the entire horizontal domain) potential temperature profi les of S150 and S30 at roughly the same time in the morning. S30 has developed a profi le that is more than 2 K cooler than S150 throughout most of the CBL. S30 also displays the warmest potential temperature near the surface. The net result is

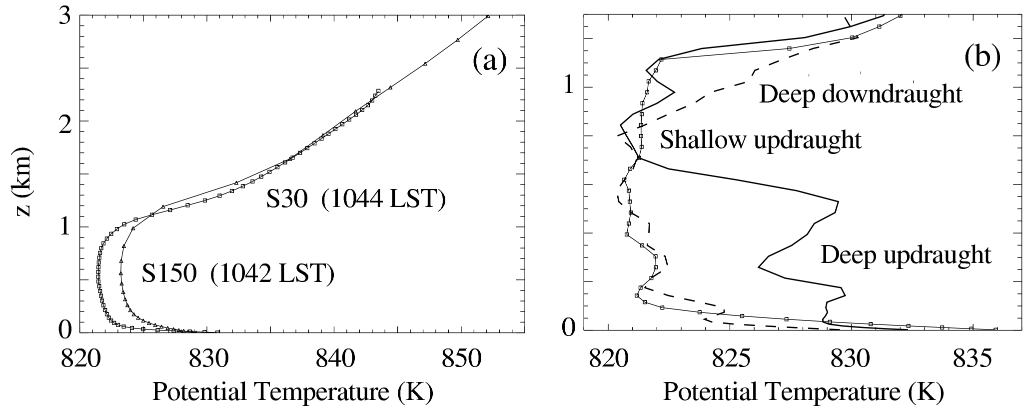


Figure 4. Potential temperature (using a reference pressure of 1000 hPa): (a) Comparison of mid-morning mean profiles. (b) Several representative, instantaneous S150 profiles at 1042 LST.

that S30 is significantly more superadiabatic at low levels than S150. Also, note that S30 exhibits a slightly shallower CBL than S150. In both simulations, the mean profile is superadiabatic for fully half of the depth of the CBL, implying that convection is not efficient enough to overcome radiative heating from below. This structure is deceiving, however, since most of the domain is populated by downdraughts whose potential temperature profiles are nearly adiabatic throughout most of the CBL (Fig. 4b). The extreme profiles of the narrow and deep large-scale updraughts are solely responsible for the shape of the mean profile. The profile through a shallow updraught in the interior of a convective cell differs from the downdraught profile only in that the lowest levels are very warm compared to even the deep updraught. Also note in Fig. 4b that the CBL depth in the downdraught is significantly less than in the two updraught profiles. Finally, the shape of the deep updraught profile indicates that the buoyant fluid is able to rise relatively adiabatically and unentrained (i.e., without mixing much with cooler fluid) through much of the depth of the CBL.

The Mars LES work of Odaka (2001) utilizes a 2-D anelastic numerical model with no radiatively active atmospheric dust, but nevertheless may be qualitatively compared to the present results. The large-scale structure of the convective eddies are quite similar, even though those of Odaka exhibit a greater vertical extent (10 km). The approximate maximum wind speeds seen by Odaka $\{\max(u, v) \approx 20$ m s$^{-1}$, $w \approx 30$ m s$^{-1}\}$ are roughly twice the wind magnitudes seen in either S30 or S150. However, these differences may be due in part to the 2-D nature of Odaka's work, as 2-D LES lack the ability to stretch vorticity. Preliminary MRAMS 2-D simulations using the present SGS formulation are seen to exhibit a deeper CBL and stronger winds than a corresponding 3-D simulation. Additionally, the mean potential temperature profiles of Odaka's results reveal a superadiabatic layer several hundred meters in depth (bounded by the surface), which compares well with MRAMS results (Fig. 4a).

(ii) *Vertical convective vortices.* Convective vortices known as dust devils are known to be common across plains during the daytime on Mars (Ryan and Lucich 1983; Thomas and Gierasch 1985; Murphy and Nelli 2002). Specimens as large as 1 km in width and 7 km tall have been seen in orbital imagery. Viking Lander and Mars Pathfinder meteorology instruments have recorded several suspected small dust devils passing over or near them (Schofield *et al.* 1997). Small dust devils have also been found in Mars Pathfinder lander imagery (Metzger *et al.* 1999). Given dust devils' often large size and apparent ubiquity at many places on Mars, it seems probable that they may be modeled in a Mars LES simulation. An LES such as S30 or even S150 should in principle be able to capture these atmospheric phenomena.

It is important to realize that a given dust devil circulation may not be visible to the unaided eye if there is no dust to entrain, the circulation does not extend fully to the surface, or if the circulation is too weak to entrain dust. In such cases, the circulation is more generally referred to as a vertical convective vortex. Also, the fine details of the dust devil circulation, especially near the ground, occur at quite small scales, and thus will not be resolved in any current LES. Finally, the structure, dynamics, and evolution of dust devils on both Earth (Sinclair 1969, 1973) and Mars are not well known. The large size of Martian dust devils may enable them to be simulated and studied with greater ease and the results applied by analogy to the study of the often much smaller terrestrial variety.

Additionally, both S30 and S150 simulation results contain abundant vertical convective vortices at many different spatial scales (several kilometers to several hundred meters in diameter) throughout the convective day that do not extend sufficiently near the surface (within about 100 meters) to be considered dust devils. In fact, the candidate dust devil circulations appear to comprise but a small subset of the total population of CBL vertical vortices. Thus these observationally "invisible" vortices appear to be an important part of the overall CBL structure on Mars {the work of Kanak *et al.* (2000) suggests a similar reality in the terrestrial CBL}. Preliminary examinations of the LES results appear to indicate that the vorticity of the simulated vertical convective vortices (including dust devils) is first generated baroclinically along updraught lines as horizontal relative vorticity, then concentrated (via horizontal convergence), tilted into the vertical, and stretched at the convective cell vertices.

Surface-based convective vortices (i.e., dust devil candidates or DDC) were found in both S30 and S150, beginning shortly after resolved-scale convection initiated and ending when the large-scale convection began to collapse. It must be noted that S150 and S30 utilize no dust lifting parametrization, and thus do not provide any quantitative way of determining whether a given convective vortex in the model solution should be termed a dust devil. The strongest and largest vertical vortices occurred during the early afternoon, when convection is at its maximum intensity. The DDC vertical vortices nearly always occurred along large-scale convective cell boundaries (updraughts), and the most intense of these vortices occurred at the vertices of the polygonal convective cell pattern. Near-surface wind speeds in the modeled DDC vortices were local maxima (on the order of 10 m $s^{-1}$), but not significantly greater than speed maxima caused by larger-scale processes. Distinct negative pressure perturbations (up to about 2 Pa) were associated with all of the mature DDC vortex circulations (as in Rafkin *et al.* 2001). The magnitude of this pressure drop compares well (after considering the difference in ambient atmospheric pressure) with measurements of Earth dust devils which exhibit perturbations of about 2 hPa. Calculations performed for a number of the modeled DDC circulations indicated that they are very nearly cyclostrophically balanced, with no obvious preferred direction of rotation. Many of the modeled DDC vortex circulations were found to attain heights of 60% of the CBL depth or more.

An example of a simulated DDC vertical convective vortex is shown in the next several figures. Figure 5a is a plot of the horizontal streamlines (1.9 m; the mean wind has been subtracted from the wind components) for a vortex that was present in S30 at 1112 LST. Note that convective vortices at this time of day are not near their peak intensity and size. The anticyclonic vortex is approximately 200 m wide at its base,

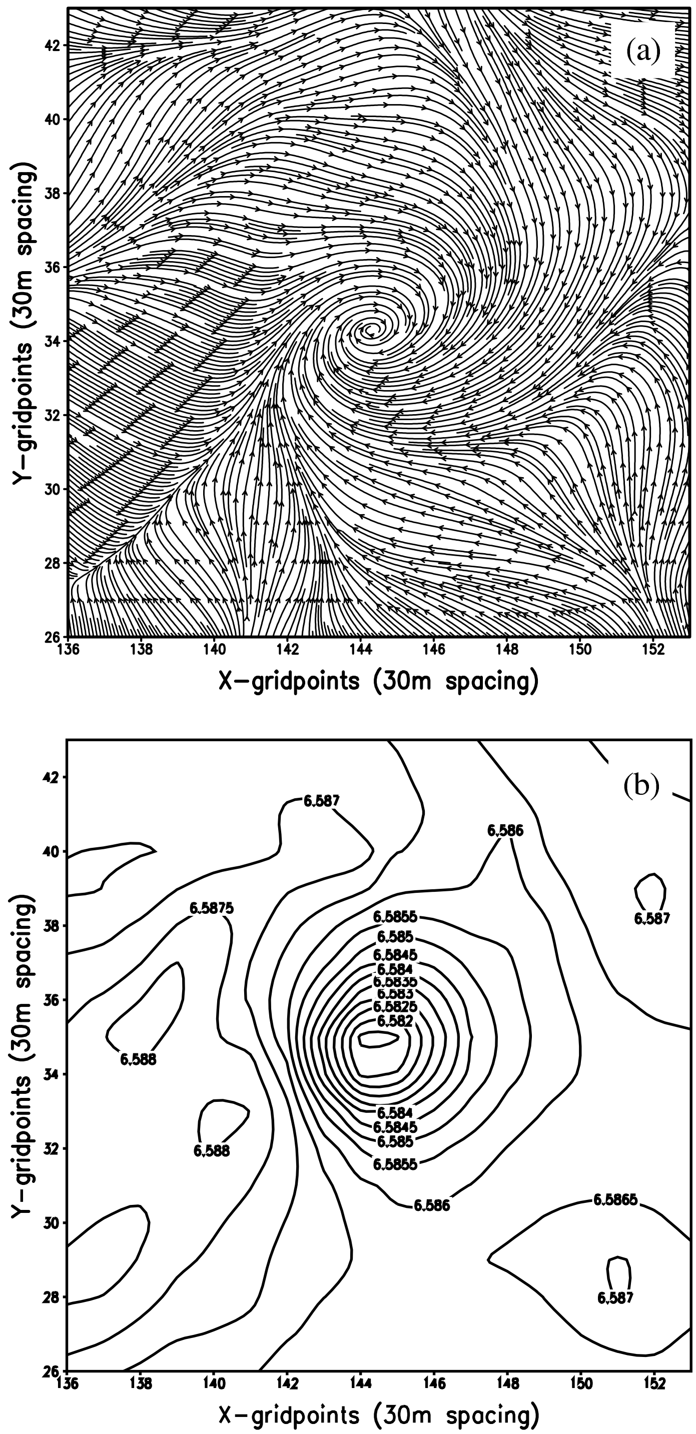


Figure 5. Horizontal cross-sections of a S30 convective vortex at 1112 LST and $z = 1.9$ m: (a) streamlines (mean wind removed); and (b) contours of pressure (hPa).

and widens and tilts toward the northeast somewhat with height. This vortex is only about 500 m deep, and if it were dust-laden, an observer would likely describe it as a wedge-type dust devil. Figure 5b illustrates the perturbation imposed on the total pressure field by the same vortex, which is quite small (about 0.55 Pa), but nevertheless is unambiguously present. This vortex lies along and is embedded in one of the narrow, quasi-linear updraught features. Due to a mean west to east wind, the northern half of this vortex exhibits the most intense wind (constructive interference). A west-east vertical cross-section of three-dimensional relative vorticity magnitude through the vortex is shown in Fig. 6a. The vortex clearly tilts with height. Figure 6b shows a similar cross-section of vertical velocity, illustrating how the convective vortex is embedded in a much larger-scale buoyant plume. Note that the maximum vertical velocity is located along the leading edge of the vortex (movement is from left to right), whereas the trailing edge is composed of a much weaker updraught.

### (*b*) *Turbulent statistics*

In light of the fact that the CBL is rife with many similar, ever-changing three-dimensional structures, it is instructive to compute a number of statistics about the flow (e.g., covariances, variances, skewness, mean profiles). For a detailed description of the statistical methods and assumptions used here, refer to Chapter 2 of Stull (1988). Such statistics provide a two-dimensional view (height and time) of the overall effects of the complex convective flows. All turbulent statistics presented here are computed as a single vertical profile for each model output time, with each profile point being assigned the average of that quantity over the entire horizontal domain at that level.

A time-height plot of the covariance of vertical velocity and temperature (a quantity proportional to the turbulent heat flux) from S150 is shown in Fig. 7a. Clearly, resolved-scale convection does not initiate in S150 until after 0930 LST. The entrainment zone above the CBL is plainly evident, growing deeper and more intense as the convective elements become larger and more energetic. The maximum value of 1.42 K m s$^{-1}$ is reached at 1300 LST (just after the time of maximum insolation), and is nearly an order of magnitude greater than maximum values measured in terrestrial desert atmosphere studies such as Schneider (1991). However, the maximum actual thermal energy flux, which is obtained by multiplying the covariance by the air density and heat capacity, is nearly an order of magnitude less than that on Earth, owing to the Martian air density being nearly two orders of magnitude smaller than on Earth. Since Mars receives approximately half the terrestrial amount of solar insolation, the Martian CBL must be more vigorous and deeper than the terrestrial CBL, due to the fact that the Martian atmosphere is so much less efficient at transporting heat. More intriguing is the presence in the mean statistics of what appear to be regular pulses of convective activity (especially evident in the entrainment zone; several can be seen in Fig. 7a – three between 1000 and 1100 LST, and two others centered at 1300 and 1415 LST) that become more intense but less frequent as the day passes. This suggests that all (or at least most) of the convective cells in the domain are involved in a concerted (i.e., not random) cycle of overturning. Finally, the amount of vertical heat transport diminishes gradually throughout the afternoon, until convection collapses completely sometime after 1700 LST.

The time-height profile of S150 turbulent kinetic energy (TKE) provides a similar perspective (not shown). The maximum depth of the CBL, when defined as the region of relatively high TKE bounded by the ground, is about 6 to 7 kilometers. The MRAMS TKE values are two to three times greater than in the typical terrestrial desert atmosphere. The intensity of the CBL circulations is greatest at around 1400 LST. After 1600

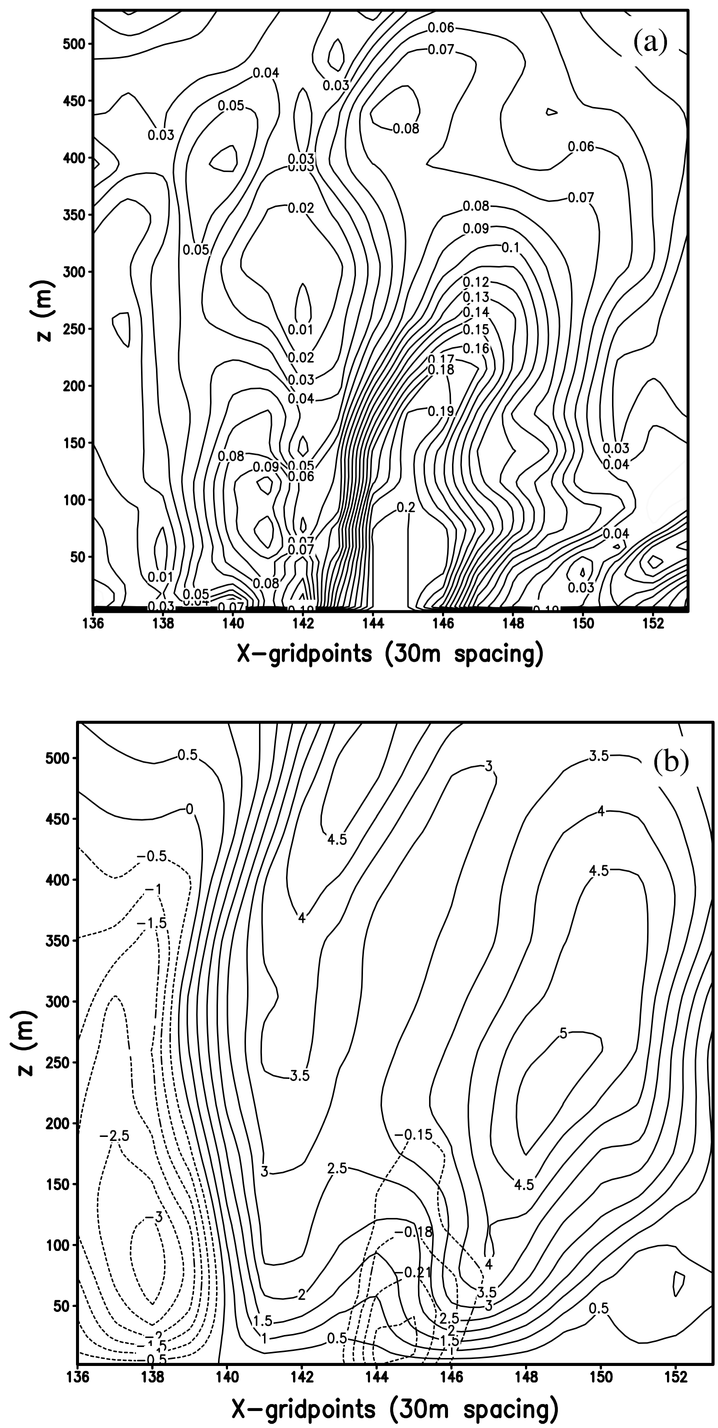


Figure 6. X-Z vertical sections ($y$ = 35) through the vortex shown in Fig. 5: (a) Three-dimensional relative vorticity magnitude (rad $s^{-1}$); and (b) vertical velocity (m $s^{-1}$, solid contours), dashed contours in lower center are relative vertical vorticity – intended only to show vortex location.

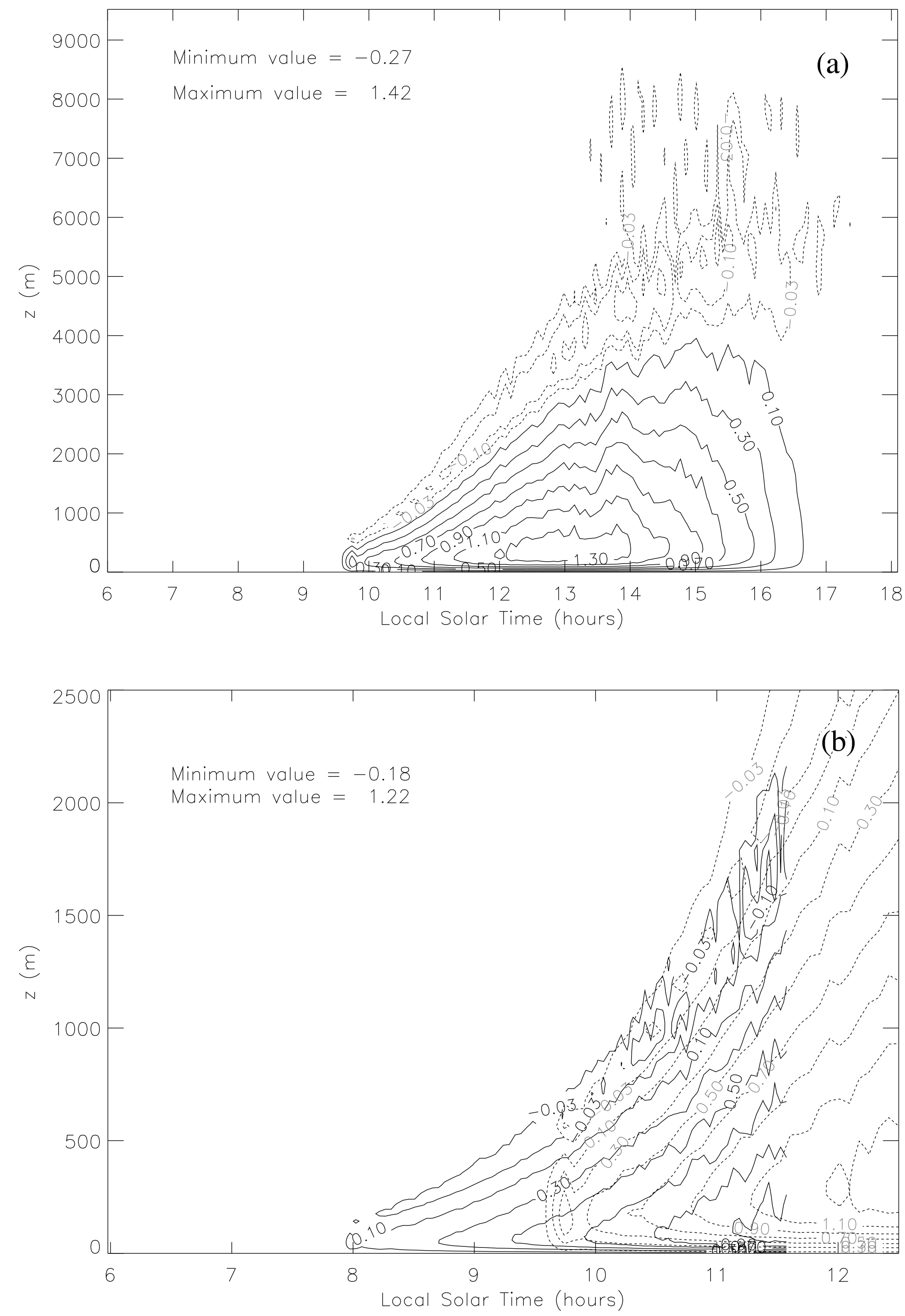


Figure 7. Time-height sections of the covariance of vertical velocity and temperature (units of K m $s^{-1}$, contours are not all equally spaced) for: (a) entire length of the S150 simulation (dashed contours indicate negative values); and (b) entire length of the S30 simulation (solid), plotted atop the corresponding S150 results (dashed).

LST, the CBL eddies rapidly lose strength and have effectively collapsed by 1730 LST. The majority of the resolved-scale turbulent kinetic energy in the Martian CBL appears to be contributed by vertical motions (as indicated by the comparison of perturbation velocity values in the vertical with those in the horizontal). This suggests that the large-scale Martian convective eddies are strongly anisotropic (in intensity).

The vertical flux of horizontal momentum (the covariance of the horizontal and vertical velocities) is not shown, but worth noting. The values of this statistic are slightly less than analogous measurements on Earth. Alternating (with time and height) positive and negative values are a puzzling feature, as they indicate periods of mean gradient and counter-gradient transport across the domain (as previously noted in Rafkin *et al.* 2001). Both individual covariances exhibit the same behavior, so the phenomenon is likely a three-dimensional process.

The next series of figures illustrate the differences between the statistics of S150 and S30. Figure 7b shows the covariance of vertical velocity and temperature from both simulations. The height of the CBL becomes slightly shallower in S30 than S150, and is believed to be the result of changes in energy transport (caused by the higher resolution grid) and not boundary effects at the model top. The most obvious difference is the location and intensity of the near-surface vertical gradient of the statistic. S30 has covariance magnitudes similar to S150, but exhibits a much stronger gradient near the surface. This difference is exemplified by the profiles of S30 and S150 covariances at approximately 0930 LST (immediately before resolved-scale convection begins in S150) shown in Fig. 8a. The S30 covariance is an order of magnitude or more greater than that of S150 throughout most of the CBL depth. Also, in S30 the SGS contribution is nearly two orders of magnitude less than the resolved one. In Earth LES studies, the resolved-scale covariance profile appears similar to that of S30. However, on Earth, the SGS contribution is quite significant near the surface, causing the total covariance profile (resolved+SGS) to be linear (negative slope) throughout the entire depth of the CBL. This profile shape indicates (via vertical heat flux divergence considerations) that convection on Earth acts to warm the atmosphere throughout the CBL. On Mars, the SGS contribution (as it is parametrized in this work) is negligible, and the lowest portion of the covariance profile exhibits a positive slope, indicating that near the surface, resolved-scale convection is acting to cool the atmosphere. To make sense of this, consider that on Earth the atmosphere receives most of its energy via conduction from the surface, while on Mars the atmosphere likely receives most of its energy via the absorption of upwelling infrared radiation from the surface {Mars' atmosphere is relatively opaque in certain regions of the infrared spectrum; see Haberle *et al.* (1993) and Savijärvi (1991)}. The role of convection in a fluid is to equalize the distribution of energy in the fluid, and as Mars' atmosphere is significantly heated internally at low levels by radiation (not just at its lowest boundary via conduction), convection would naturally act to cool the atmosphere in that region and warm the portion above.

Figure 8b shows the covariance profiles after both simulations have achieved resolved-scale convection. It clearly shows a difference in CBL depth and in near-surface structure between S30 and S150. A comparison of S30 and S150 TKE statistics reveals a similar situation. This contrast is likely due to inadequacies of the SGS parametrization, as the total S150 covariance should be similar to the S30 results at the same time and height if the SGS scheme were performing perfectly. Unfortunately, a parametrization is, by its very nature, an approximation, and therefore will likely never perfectly represent its real-life or analytical counterpart. SGS parametrizations also do not perform ideally on Earth (e.g., Mason 1989), but this fact does not prevent terrestrial LES studies from drawing many meaningful conclusions. Thus, similar conclusions may

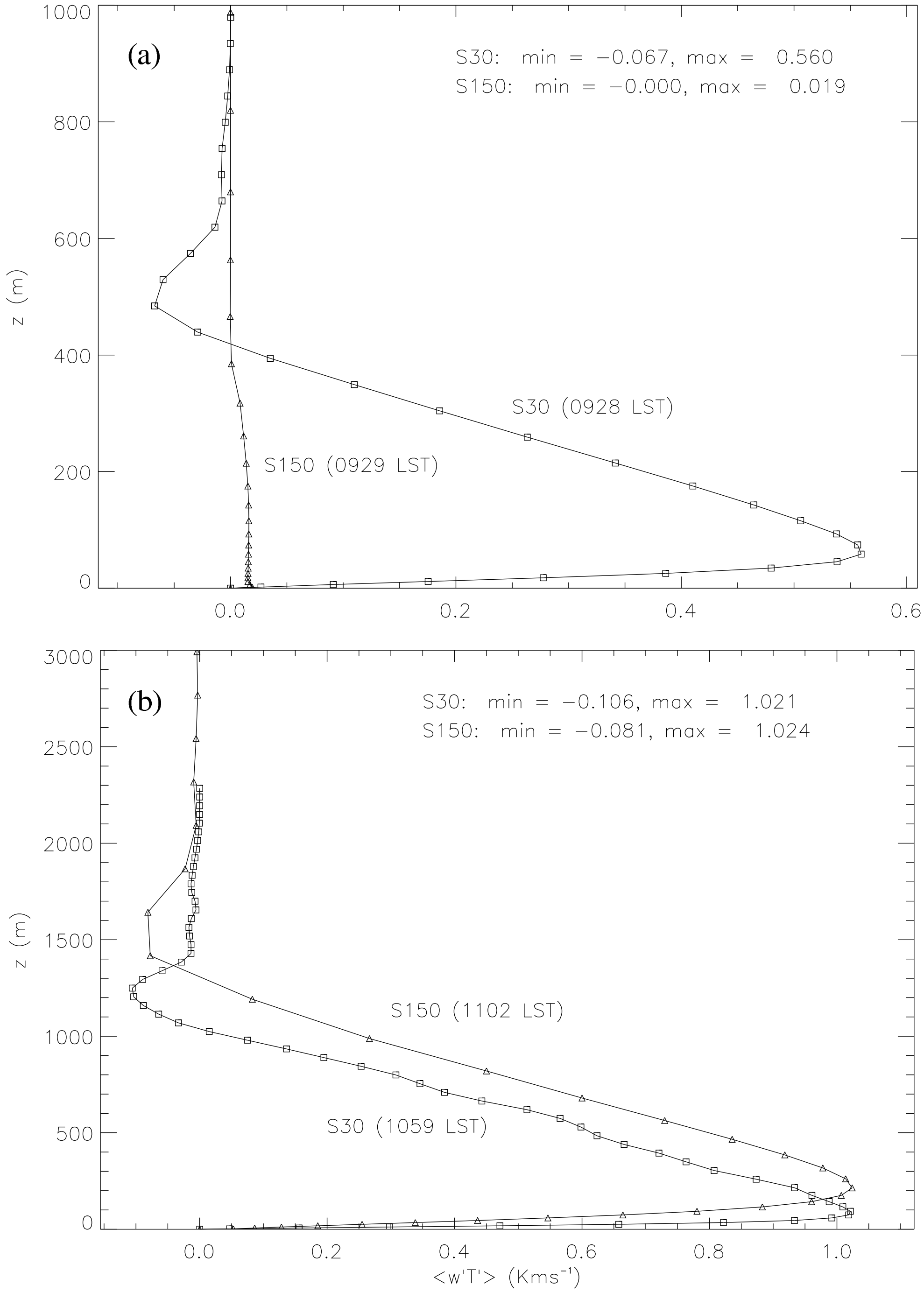


Figure 8. Comparisons of the S150 and S30 vertical profiles of the covariance of vertical velocity and temperature (sum of resolved-scale and subgrid-scale contributions) for: (a) mid-morning; and (b) late-morning.

be also be made about the Mars CBL if the level of parametrization imperfection appears to be of minimal importance to the robustness of key CBL structure and statistics. Such appears to be the case, as the maximum and minimum values of the covariance (Fig. 8b) in both S30 and S150 are nearly identical, as are the qualitative shapes of the profiles. Furthermore, the large-scale convective structure of S30 and S150 are quite similar, and the MRAMS LES results compare well with high-resolution spacecraft images of small-scale atmospheric phenomena (e.g., convective clouds), providing a measure of qualitative model validation.

Figure 9b shows the vertical velocity skewness profiles of S30 and S150. Assuming that the domain mean vertical velocity at each level is zero (in reality it is quite small), a positive value of this statistic indicates that updraughts are narrower than surrounding downdraughts, and vice versa. The vertical velocity skewness is positive throughout most of the CBL, and has a maximum near the top of the CBL. Gravity (buoyancy) waves propagating along the top of the CBL are the reason for the sudden decrease above the maximum, since they have roughly equal areas of upward and downward velocity. Near the surface, the skewness becomes distinctly negative, indicating a tendency for narrow downdraughts and broad rising motion there. These profiles are quite similar in all respects to Earth LES results, though those terrestrial results do not agree well with Earth observations (Moeng and Rotunno 1990). Also note the effect grid resolution has on the skewness profiles. Figure 9a shows a time-height plot of the S150 vertical velocity skewness. It shows that throughout the convective day, the skewness profile is quite consistent until about 1630 LST, when skewness aloft decreases rapidly, indicating the collapse of the narrow updraughts. Also visible at approximately 1715 LST is the reversal of the near-surface skewness from negative to positive, indicating broad downward motion and narrow regions of upward motion. Nearly simultaneously, the skewness aloft also switches sign. These reversals appear to indicate the onset of the nocturnal ABL processes.

### (*c*) *Comparison to Mars Pathfinder (MPF) data*

The measured MPF temperature and wind time series have a rather large variance during the day. This has been interpreted as primarily being the effects of daytime convection at the MPF site. If that is the case, the variance of the temperature and wind time series from the present LES simulations (at the MPF site) should compare well with the lander dataset. It is important to note, however, that with the possible exception of temperature, the mean magnitudes of the LES quantities cannot be expected to match those of the MPF observations, due to the partially idealized nature of the present LES (i.e., no topography or mesoscale pressure gradients). LES results are from S150 and are plotted every 300 s. The time resolution of the MPF data vary, but are generally of higher time resolution than the LES results presented here. Finally, though the S30 results will not be shown here, the variation that they exhibit is slightly greater than that of the S150 results. Also, the MPF wind data shown in Fig. 10 have not yet been fully calibrated. Even so, it is likely that most values are close to the fully calibrated values.

Figure 10a compares observed and modeled temperature at a height of 1.27 m above the surface. MRAMS temperatures here are simply linearly extrapolated from the lowest model level of 1.9 m. The MRAMS values are slightly colder than the MPF data, but do exhibit a variance of about 4 K (observed value is about 10K during mid-day).

Modeled and observed wind speeds are shown in Fig. 10c. Again MRAMS exhibits a sizable amount of variation (about 7 m $s^{-1}$) due to convective motions. Also note the steep drop (after the 25.7 time graduation) in the wind magnitude and variability after the large-scale convection collapses (seen also in the MPF dataset). A comparison of

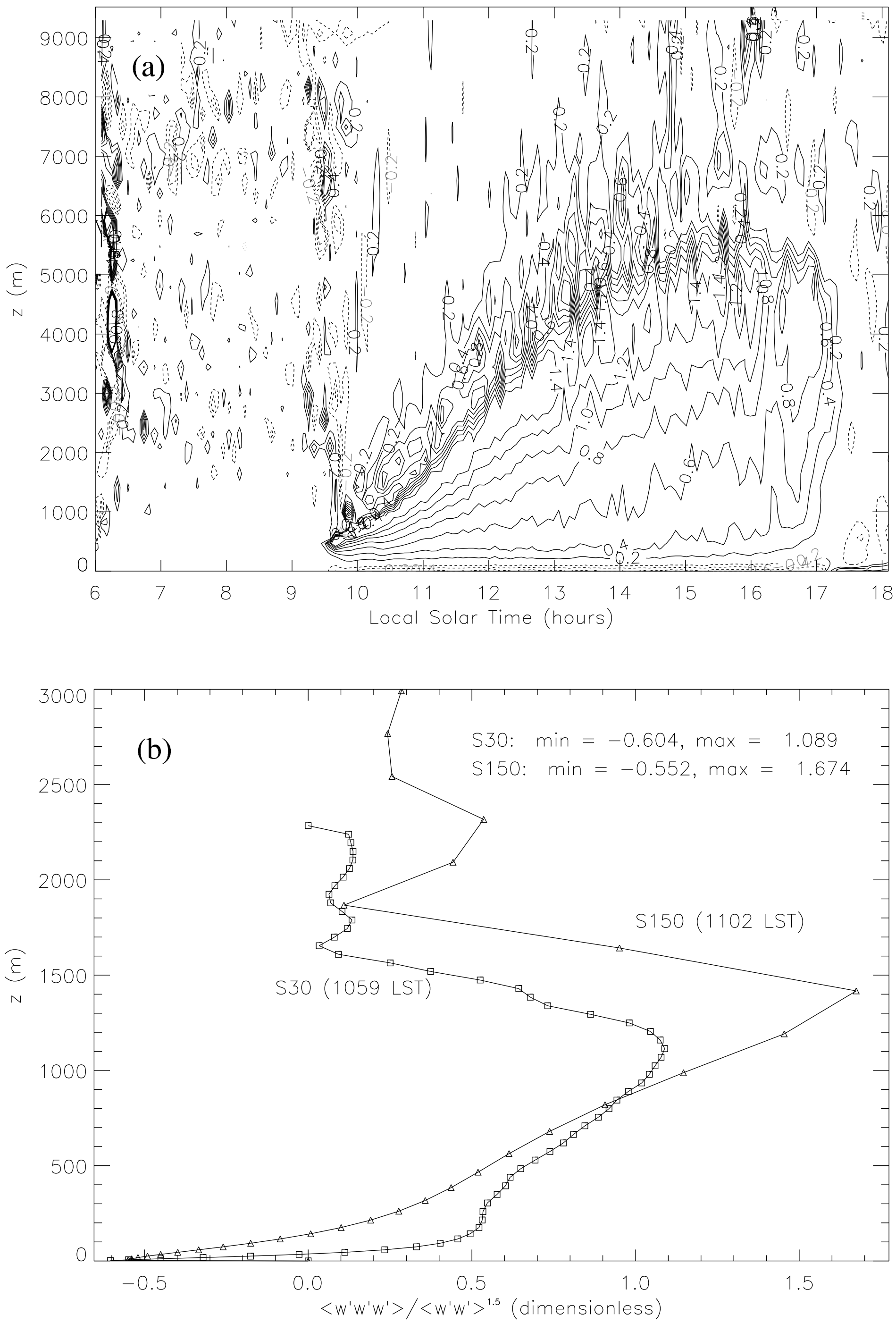


Figure 9. Vertical velocity skewness (dimensionless): (a) S150 time-height section (dashed contours denote negative values); and (b) comparison of late-morning S30 and S150 profiles.

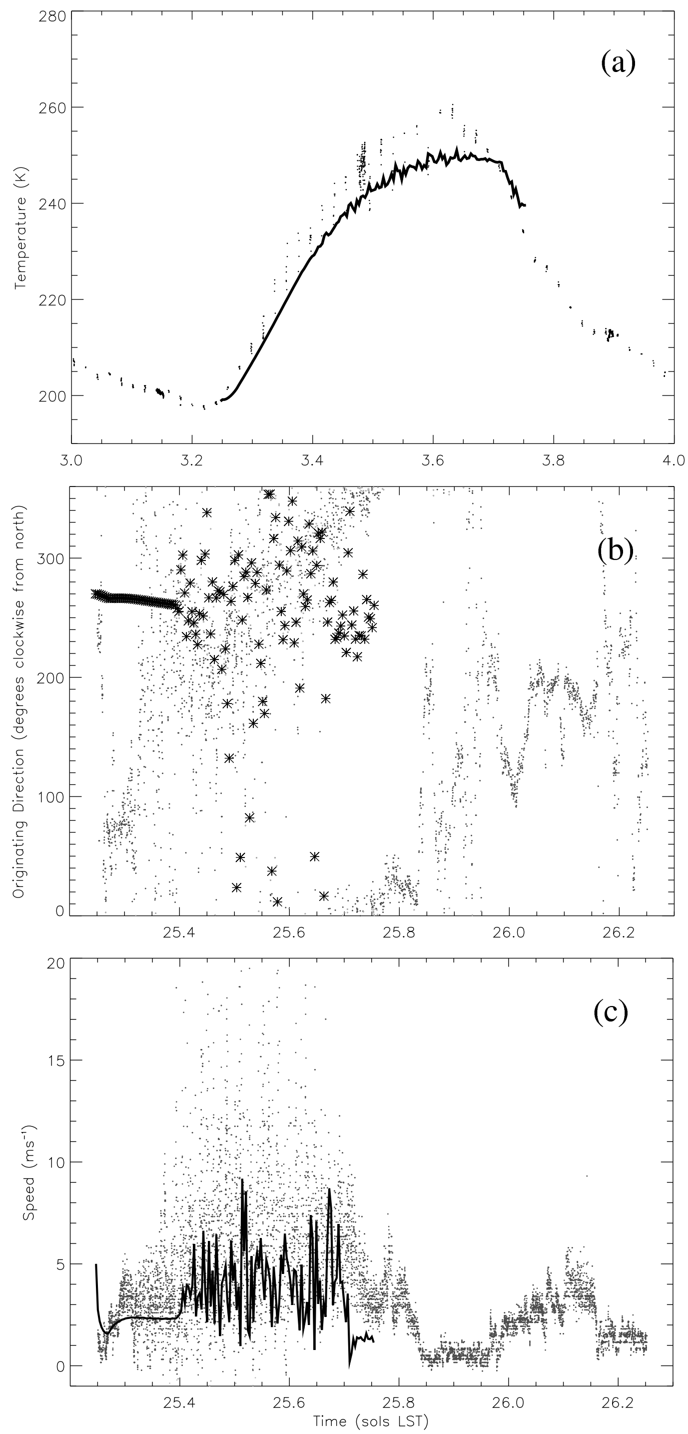


Figure 10. Time series comparison of 1.27 m Mars Pathfinder (MPF) measurements (wind data provided by Dr. J. Murphy, New Mexico State University, USA) and extrapolated S150 results for: (a) temperature (black points, MPF; black line, S150); (b) wind direction (dark points, MPF; black asterisks, S150); and (c) wind speed (dark points, MPF; black line, S150).

modeled and observed wind direction is shown in Fig. 10b. The amount of variation in the MRAMS wind direction compares well to the MPF data. Again note that after convection collapses, the wind direction becomes much more constant (borne out in the MPF data as well).

## 4. Conclusions

Two LES of the Martian atmosphere were performed using horizontal grid spacings of 30 and 150 m. The convective boundary layer of Mars was found to exhibit large-scale structures and turbulent statistics outwardly similar to those in Earth's CBL. Numerous convective vortices (including possible dust devils) were also present in both simulations. MRAMS LES results compared well with high-resolution spacecraft images of small-scale atmospheric phenomena, such as convective clouds, which attest to the existence of certain CBL structures. However, several key differences between the CBL of Mars and Earth were noted: First, the lower atmosphere of Mars likely receives energy from the Sun primarily through the absorption of upwelling infrared radiation from the surface. This causes convection on Mars to cool the lower levels of the CBL and heat the remainder, whereas on Earth convection heats the entire CBL. Secondly, Mars' lesser gravity, much lower atmospheric density (thus much less heat transport efficiency), and comparable amount of insolation (roughly half that of Earth) result in anisotropic convection that is several times deeper and more intense than that on Earth. Finally, the scaling constants (see Section 2a) used in the lightly modified terrestrial subgrid-scale turbulence scheme employed by this study required significant reduction (to less than one-fourth their usual terrestrial values) in order for resolved-scale convection to initiate at all.

A suggested cause for the latter conclusion: the presence of non-dissipative, energetic turbulence ("large eddies") that occurs at considerably smaller scales than on Earth. In essence, the "large eddies" of the Mars atmosphere may exist in a wider spatial range than that of Earth (i.e., approximately 0.2 - 3 km on Earth, $<$0.2 - 8 km on Mars). Additionally, even though the assumptions made by the SGS parametrization are largely quite general (e.g., isotropic turbulence, parametrized turbulence acts to dissipate energy, etc.), they will improperly represent the effects of such "large eddies" on the atmospheric energy budget. In light of this, it is surmised that the terrestrial SGS scheme scaling constants (Deardorff 1980) should become approximately valid at some non-molecular scale on Mars (possibly significantly smaller than 30 m). Future work will investigate these issues further.

The ABL is a complex and important region of the Mars atmosphere that should not be ignored nor treated as a perfect analog of Earth's ABL. This study both elucidated details of and raised further questions about a partially idealized, representative Mars CBL. Also, after further effort, spacecraft images may be used to estimate Mars CBL depths and structure over large portions of the planet without expressly conducting time- and resource-intensive Large Eddy Simulations. Additional future work should strive to use relevant spacecraft data and more realistic LES (e.g., incorporate topography, seasonality, mesoscale atmospheric forcings, 3-D radiative transfer, full diurnal cycle) to further constrain our knowledge of the Mars ABL.

## Acknowledgements

The authors wish to thank Dr. James Murphy of New Mexico State University (USA), for kindly providing high-resolution Mars Pathfinder wind data for comparison to the Mars LES solution. This work was supported by National Aeronautics and Space Administration (USA) (NASA) Mars Data Analysis Program (MDAP) grant No. NAG5-9500. Lastly, the comments of two anonymous reviewers are appreciated. They provided insightful comments that improved this manuscript.

## REFERENCES


| | | |
|---|---|---|
| Atkinson, B. W. and Zhang, J. W. | 1996 | Mesoscale shallow convection in the atmosphere, *Rev. Geophys.,* **34,** 403–431 |
| Blumsack, S. L., Gierasch, P. J. and Wessel, W. R. | 1973 | An analytical and numerical study of the Martian planetary boundary layer over slopes. *J. Atmos. Sci.,* **30,** 66–82 |
| Briggs, G., Klaasen, K., Thorpe, T. and Wellman, J. | 1977 | Martian dynamical phenomena during June-November 1976: Viking Orbiter imaging results. *J. Geophys. Res.,* **82,** 4121–4149 |
| Deardorff, J. W. | 1972 | Numerical investigation of neutral and unstable planetary boundary layers. *J. Atmos. Sci.,* **29,** 91–115 |
| | 1980 | Stratocumulus-capped mixed layers derived from a three-dimensional model. *Bound. Layer Meteor.,* **18,** 495–527 |
| Dörnbrack, A. | 1997 | Broadening of convective cells. *Q. J. R. Meteorol. Soc.,* **123,** 829–847 |
| Fiedler, B. H. and Khairoutdinov, M. | 1994 | Cell broadening in three-dimensional thermal convection between poorly conducting boundaries: Large eddy simulations. *Beitr. Phys. Atmos.,* **67,** 235–241 |
| Goody, R. M. and Belton, M. J. S. | 1967 | Radiative relaxation times for Mars. *Plan. Space Sci.,* **15,** 247–256 |
| Haberle, R. M., Houben, H. C., Hertenstein, R. and Herdtle, T. | 1993 | A boundary-layer model for Mars: Comparison with Viking lander and entry data. *J. Atmos. Sci.,* **50,** 1544-1559 |
| Haberle, R. M., Joshi, M. M., Murphy, J. R., Barnes, J. R., Schofield, J. T., Wilson, G. W., Lopez-Valverde, M., Hollingsworth, J. L., Bridger, A. F. C. and Schaeffer, J. | 1999 | General circulation model simulations of the Mars Pathfinder atmospheric structure investigation/meteorology data. *J. Geophys. Res.,* **104,** 8957–8974 |
| Hadfield, M. G., Cotton, W. R. and Pielke, R. A. | 1991 | Large-eddy simulations of thermally-forced circulations in the convective boundary layer. Part I: A small-scale circulation with zero wind. *Boundary-Layer Meteorol.,* **57,** 79–114 |
| Kanak, K., Lilly, D. and Snow, J. | 2000 | The formation of vertical vortices in the convective boundary layer. *Q. J. R. Meteorol. Soc.,* **126,** 2789–2810 |
| Malin, M. C. and Edgett, K. S. | 2001 | The Mars Global Surveyor Mars Orbiter Camera: Interplanetary Cruise through Primary Mission. *J. Geophys. Res.,* **106(E10),** 23429–23570 |
| Mason, P. J. | 1989 | Large-eddy simulation of the convective atmospheric boundary layer. *J. Atmos. Sci.,* **46,** 1492–1516 |
| Metzger, S. M., Carr, J. R., Johnson, J. R., Parker, T. J. and Lemmon, M. | 1999 | Dust devil vortices seen by the Mars Pathfinder camera. *Geophys. Res. Lett.,* **26,** 2781–2784 |
| Michaels, T. I. | 2002 | 'Large eddy simulation of atmospheric convection on Mars'. M.Sc. thesis, San Jose State University, USA |
| Moeng, C. H. and Rotunno, R. | 1990 | Vertical-velocity skewness in the buoyancy-driven boundary layer. *J. Atmos. Sci.,* **47,** 1149–1162 |
| Moeng, C. H. and Sullivan, P. P. | 1994 | A comparison of shear- and buoyancy-driven planetary boundary layer flows. *J. Atmos. Sci.,* **51,** 999–1022 |
| Murphy, J. R. and Nelli, S. | 2002 | Mars Pathfinder Convective Vortices: Frequency of Occurrence *Geophys. Res. Lett.,* **29(23),** 2103, doi:10.1029/2002GL015214 |
| Odaka, M. | 2001 | A numerical simulation of Martian atmospheric convection with a two-dimensional anelastic model: A case of dust-free Mars. *Geophys. Res. Lett.,* **28,** 895–898 |
| Odaka, M., Nakajima, K., Takehiro, S., Ishiwatari, M. and Hayashi, Y.-Y. | 1998 | A numerical study of the Martian atmospheric convection with a two dimensional anelastic model. *Earth, Planet and Space,* **50,** 431–437 |
| Pollack, J. B., Leovy, C. B., Mintz, Y. and Van Camp, W. | 1976 | Winds on Mars during the Viking season: Predictions based on a general circulation model with topography. *Geophys. Res. Lett.,* **3,** 479–483 |

Rafkin, S. C. R, Haberle, R. M. and Michaels, T. I. 2001 The Mars Regional Atmospheric Modeling System: model description and selected simulations. *Icarus,* **151,** 228–256

Ryan, J. A. and Lucich, R. D. 1983 Possible dust devils: Vortices on Mars. *J. Geophys. Res.,* **88,** 11005–11011

Savijärvi, H. 1991 Radiative fluxes on a dustfree Mars. *Contrib. Atmos. Phys.,* **64,** 103-112

1995 Mars boundary layer modeling: Diurnal moisture cycle and soil properties at the Viking Lander 1 site. *Icarus,* **117,** 120–127

1999 A model study of the atmospheric boundary layer in the Mars Pathfinder lander conditions. *Q. J. R. Meteorol. Soc.,* **125,** 483–493

Savijärvi, H. and Siili, T. 1993 The Martian slope winds and the nocturnal PBL jet. *J. Atmos. Sci.,* **50,** 77–88

Schmidt, H. and Schumann, U. 1989 Coherent structure of the convective boundary layer derived from large-eddy simulations. *J. Fluid Mech.,* **200,** 511–562

Schneider, J. M. 1991 'Dual Doppler Measurement of a Sheared Convective Boundary Layer'. PhD thesis, The University of Oklahoma, Norman, USA

Schofield, J. T., Barnes, J. R., Crisp, D., Haberle, R. M., Larsen, S., Magalhaes, J. A., Murphy, J. R., Seiff, A., Wilson, G. 1997 The Mars Pathfinder atmospheric structure investigation/meteorology (ASI/MET) experiment. *Science,* **278,** 1752–1758

Sinclair, P. C. 1969 General characteristics of dust devils, *J. Appl. Meteorol.,* **8,** 32-45

1973 Lower structure of dust devils, *J. Atmos. Sci.,* **30,** 1599-1619

Stull, R. B. 1988 *Boundary Layer Meteorology.* Kluwer Academic Publications, Dordrecht, The Netherlands

Sutton, J. L., Leovy, C. B. and Tillman, J. E. 1978 Diurnal variation of the martian surface layer meteorological parameters during the first 45 sols at two Viking lander sites. *J. Atmos. Sci.,* **35,** 2346–2355

Thomas, P. and Gierasch, P. J. 1985 Dust devils on Mars. *Science,* **230,** 175–177

Walko, R. L., Cotton, W. R. and Pielke, R. A. 1992 Large-eddy simulation of the effects of hilly terrain on the convective boundary layer. *Boundary-Layer Meteorol.,* **58,** 133–150

Wang, H. and Ingersoll, A. P. 2002 Martian clouds observed by Mars Global Surveyor Mars Orbiter Camera. *J. Geophys. Res.,* **107(E10),** 5078, doi:10.1029/2001JE001815

Ye, Z. J., Segal, M. and Pielke, R. A. 1990 A comparative study of daytime thermally induced upslope flow of Mars and Earth. *J. Atmos. Sci.,* **47,** 612–628